nature neuroscience

ARTICLES

https://doi.org/10.1038/s41593-018-0289-8

Tau impairs neural circuits, dominating amyloid-β effects, in Alzheimer models in vivo

Marc Aurel Busche[1,2*], Susanne Wegmann[1,3], Simon Dujardin[1], Caitlin Commins[1], Julia Schiantarelli[1], Naomi Klickstein[1], Tarun V. Kamath[1], George A. Carlson[4], Israel Nelken[5] and Bradley T. Hyman[1*]

The coexistence of amyloid-β (Aβ) plaques and tau neurofibrillary tangles in the neocortex is linked to neural system failure and cognitive decline in Alzheimer's disease. However, the underlying neuronal mechanisms are unknown. By employing in vivo two-photon Ca^{2+} imaging of layer 2/3 cortical neurons in mice expressing human Aβ and tau, we reveal a dramatic tau-dependent suppression of activity and silencing of many neurons, which dominates over Aβ-dependent neuronal hyperactivity. We show that neurofibrillary tangles are neither sufficient nor required for the silencing, which instead is dependent on soluble tau. Surprisingly, although rapidly effective in tau mice, suppression of tau gene expression was much less effective in rescuing neuronal impairments in mice containing both Aβ and tau. Together, our results reveal how Aβ and tau synergize to impair the functional integrity of neural circuits in vivo and suggest a possible cellular explanation contributing to disappointing results from anti-Aβ therapeutic trials.

The primary pathological hallmarks of Alzheimer's disease are extracellular plaques and intracellular neurofibrillary tangles (NFTs)[1]. The main component of plaques is the amyloid-β (Aβ) peptide, while NFTs are composed mainly of the protein tau. Autopsy and recent positron emission tomography studies revealed that the formation of plaques is spatially and temporally separated from that of NFTs: plaques first form in the neocortex and spread inward to deeper brain regions, while NFTs first form in limbic areas, from where they spread outward to the neocortex[2–4]. Several lines of evidence suggest that the propagation of tau pathology into the Aβ plaque-bearing cortex is linked to the transition from the preclinical (asymptomatic) to the clinical (symptomatic) stage of Alzheimer's disease[5–7]. While previous studies have shown that the interaction between Aβ and tau causes enhanced pathology[6–14], the functional consequences for intact neuronal circuits remain unknown. To address this question, we employed in vivo two-photon Ca^{2+} imaging of large populations of neurons in layer 2/3 of the neocortex in novel Alzheimer's disease model mice that display spatially overlapping Aβ and tau pathologies in the cortex, similar to Alzheimer's disease patients.

Results

Aβ promotes neuronal hyperactivity while tau suppresses activity. We began by monitoring action potential-related spontaneous Ca^{2+} transients[15,16] in GCaMP6f-expressing cortical layer 2/3 neurons of APPswe:PS1ΔE9 (henceforth APP/PS1) transgenic mice that overexpress human Aβ and develop only Aβ plaques, but no cytosolic tau pathology. APP/PS1 mice and all other mice used in this study are on the same FVBB6F1 genetic background (see Methods and Life Sciences Reporting Summary for details regarding the breeding strategy). In agreement with previous results[17–20], we detected hyperactivity of layer 2/3 neurons in 6–12-month-old plaque-bearing APP/PS1 mice (mean age 8.4 months; see also Supplementary Figs. 1 and 2a for details regarding age distributions and the rationale for pooling functional neuronal data from mice at this 6–12-month age range) when compared to their wild-type controls (mean age 8.4 months; Fig. 1a–h). We then analyzed layer 2/3 neuronal activity in age-matched rTg4510 transgenic mice that express aggregating human tau^{P301L} and display NFTs but no Aβ pathology (Fig. 1c). In stark contrast to the results obtained with APP/PS1 mice, in all nine rTg4510 mice (mean age 8.4 months) examined, there was a strong reduction of cortical activity levels (Fig. 1c–h; linear mixed effects model (LMEM) for log rates on genetic background, $F(2,4351)=132$, $P=1.2\times10^{-56}$; all post hoc comparisons between genotypes (controls, APP/PS1, rTg4510) were highly significant, $P<10^{-6}$). Detailed analysis of all recorded neurons revealed that, relative to controls and APP/PS1 mice, there was a 3.6-fold and 5.8-fold increase in the proportion of silent neurons in the rTg4510 mice (Fig. 1i), but virtually no neuronal hyperactivity (Fig. 1h). We then analyzed immunohistochemically stained brain sections from the imaged rTg4510 mice and found that NFTs were present only in 1.21% of GCaMP6f-expressing cells (18 out of 1,483 cells were double-positive for Alz50/Paired-helical filament 1 (PHF1) and green fluorescent protein (GFP); Supplementary Fig. 3), leading us to the hypothesis that tau aggregation is not necessary for neuronal silencing.

To test this hypothesis directly, we performed recordings in rTg21221 mice that overproduce non-aggregating wild-type human tau at comparable levels as rTg4510 mice but lack NFTs (Fig. 2a, right panel, and Supplementary Figs. 4 and 5). Indeed, Fig. 2b–e shows that, similar to rTg4510 mice (Fig. 1), in 6–12-month-old rTg21221 mice ($n=6$; mean age 8.9 months) there was a marked reduction of layer 2/3 neuronal activity levels (LMEM for log rates on genetic background, $F(2,4494)=183$, $P=1.6\times10^{-77}$; post hoc multiple comparisons between genotypes were $P<0.0001$), as well

[1]MassGeneral Institute for Neurodegenerative Disease, Massachusetts General Hospital, Harvard Medical School, Charlestown, MA, USA. [2]UK Dementia Research Institute, University College London, London, UK. [3]German Center for Neurodegenerative Diseases (DZNE), Berlin, Germany. [4]McLaughlin Research Institute for Biomedical Sciences, Great Falls, MT, USA. [5]Department of Neurobiology, Silberman Institute of Life Sciences and Edmond and Lily Safra Center for Brain Sciences, Hebrew University of Jerusalem, Jerusalem, Israel. *e-mail: m.busche@ucl.ac.uk; bhyman@mgh.harvard.edu

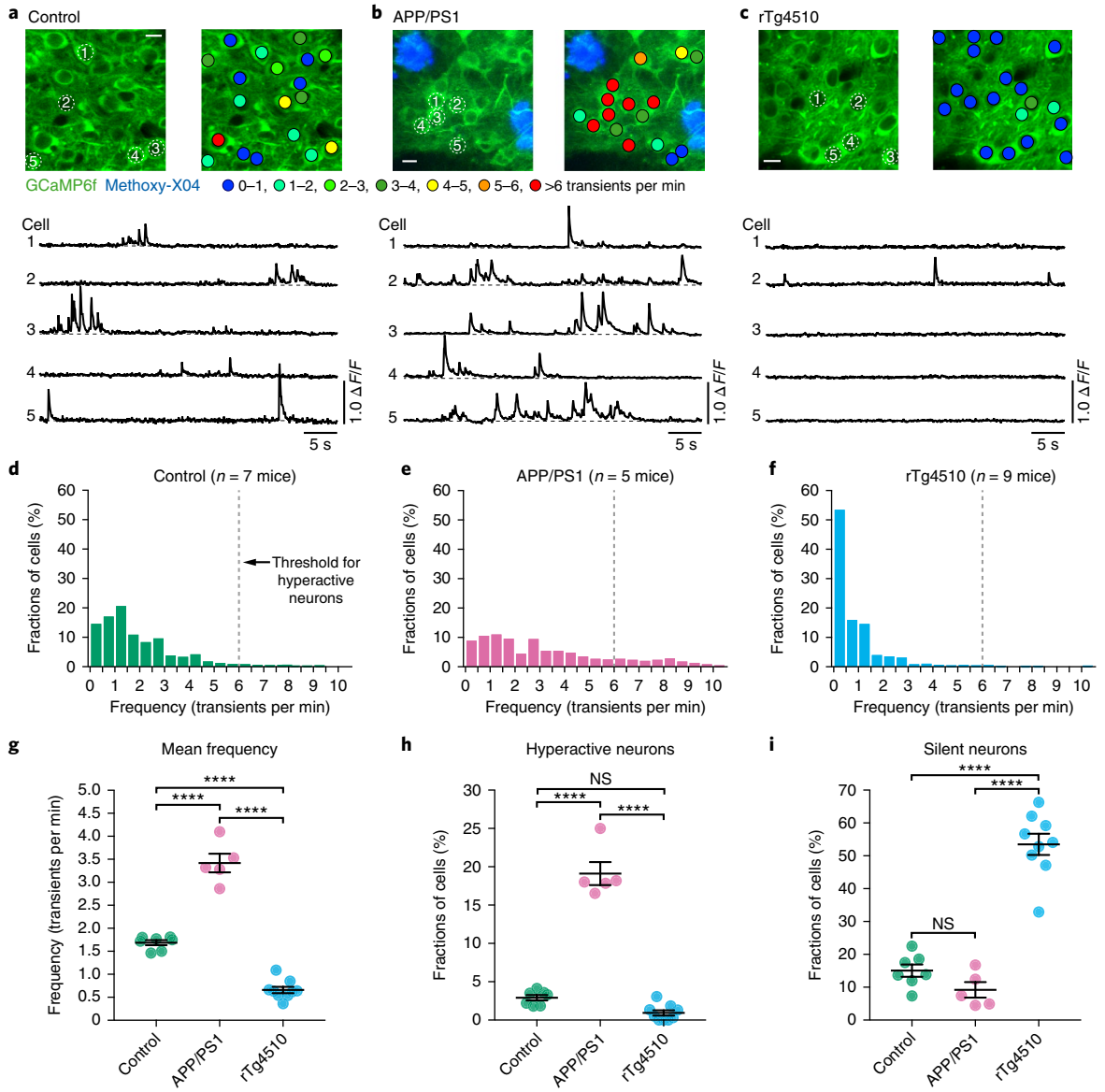

Fig. 1 | Neuronal hyperactivity in APP/PS1 mice but silencing in rTg4510 tau mice. a–c, Top, in vivo two-photon fluorescence images of GCaMP6f-expressing (green) layer 2/3 neurons in the parietal cortex and corresponding activity maps from wild-type controls (**a**), APP/PS1 (**b**), and rTg4510 (**c**) mice. In APP/PS1 mice, plaques were labeled with methoxy-X04 (blue); in the activity maps, neurons were color-coded as a function of their mean activity. Scale bars, 10 µm. Bottom, spontaneous Ca^{2+} transients of neurons indicated in the top panel. **d–f**, Frequency distributions of all recorded neurons in controls (**d**; green, $n=1{,}705$ neurons in 7 mice), APP/PS1 (**e**; magenta, $n=878$ neurons in 5 mice), and rTg4510 mice (**f**; light blue, $n=1{,}771$ neurons in 9 mice). The dashed line at 6 transients per min indicates the threshold used to identify hyperactive neurons; silent neurons exhibit 0 transients per min. **g**, Mean neuronal frequencies for controls (1.69 ± 0.05 transients per min), APP/PS1 (3.42 ± 0.20 transients per min), and rTg4510 (0.66 ± 0.07 transients per min); $F(2,18)=171.2$, $P=1.93\times10^{-12}$. All post hoc multiple comparisons between genotypes were highly significant: $P=5.42\times10^{-9}$ for controls vs. APP/PS1, $P=1.38\times10^{-6}$ for controls vs. rTg4510, and $P=1.01\times10^{-12}$ for APP/PS1 vs. rTg4510. **h**, Fractions of hyperactive neurons. Controls: 2.91 ± 0.35%, APP/PS1: 19.11 ± 1.50%, rTg4510: 0.93 ± 0.35%; $F(2,18)=176.2$, $P=1.51\times10^{-12}$. Post hoc multiple comparisons were $P=2.84\times10^{-11}$ for controls vs. APP/PS1, $P=1.64\times10^{-12}$ for APP/PS1 vs. rTg4510 and not significant, $P=0.1045$, for controls vs. rTg4510. **i**, Fractions of silent neurons. Controls: 15.05 ± 1.87%, APP/PS1: 9.20 ± 2.36%, rTg4510: 53.48 ± 3.24%; $F(2,18)=77.18$, $P=1.48\times10^{-9}$. Post hoc multiple comparisons were $P=2.02\times10^{-8}$ for controls vs. rTg4510 and $P=1.08\times10^{-8}$ for APP/PS1 vs. rTg4510 and not significant, $P=0.3972$, for controls vs.s APP/PS1. Each solid circle represents an individual animal (controls, $n=7$; APP/PS1, $n=5$; rTg4510, $n=9$) and all error bars reflect the mean ± s.e.m; the differences between genotypes were assessed by one-way ANOVA followed by Tukey's multiple comparisons test, ****$P<0.0001$. NS, not significant.

as a strong increase in the fractions of silent neurons (Fig. 2e). These results indicate that the impairment of neurons can occur independently of tau aggregation and NFT formation.

Combination of Aβ and tau leads to suppressed activity. Having demonstrated that Aβ and tau alone have markedly opposite effects on the activity status of neurons, we next asked what is the net effect of Aβ and tau together. To address this question, we performed recordings in 6–12-month-old APP/PS1 mice crossed with rTg4510 or rTg21221 mice[11,21] (Fig. 3a–c and Supplementary Fig. 6). To our surprise, neuronal hyperactivity was not only completely abolished in the resulting APP/PS1-rTg4510 ($n=8$; mean age 7.6 months) and

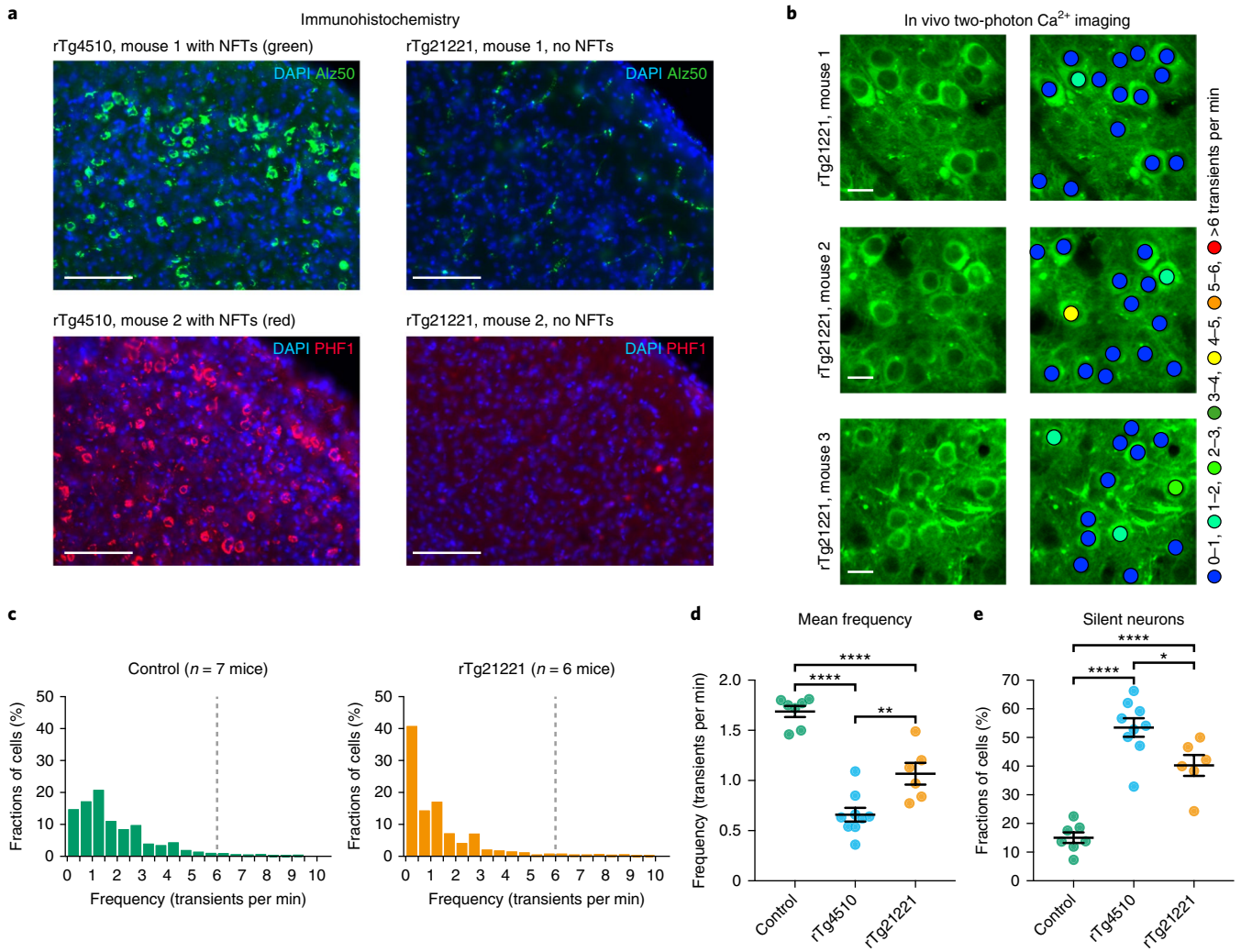

Fig. 2 | NFTs are not required for neuronal silencing. a, Coronal sections showing many Alz50-positive (top, green) and PHF1-positive (bottom, red) NFTs in the cortex of rTg4510 mice ($n=4$ mice, 8–10 sections per mouse were analyzed), but not in rTg21221 mice ($n=4$ mice, 5–12 sections per mouse were analyzed). Nuclei are visualized with DAPI (blue). Scale bars, 100 µm. **b**, In vivo two-photon fluorescence images of GCaMP6f-expressing (green) layer 2/3 neurons and corresponding activity maps from three example rTg21221 mice illustrating the marked silencing of many neurons. Scale bars, 10 µm. **c**, Frequency distributions of all recorded neurons in wild-type controls (left panel, green, $n=1{,}705$ neurons in 7 mice) and rTg21221 mice (right panel, orange, $n=1{,}021$ neurons in 6 mice). **d**, Mean frequency of silent neurons. Controls: 1.69 ± 0.05 transients per min; rTg4510: 0.66 ± 0.07 transients per min; rTg21221: 1.07 ± 0.11 transients per min. $F(2,19)=48.43$, $P=3.47\times10^{-8}$. All post hoc multiple comparisons between genotypes were significant: $P=2.01\times10^{-8}$ for controls vs. rTg4510, $P=1.00\times10^{-4}$ for controls vs. rTg21221, $P=0.0038$ for rTg4510 vs. rTg21221. **e**, Fractions of silent neurons. Controls: 15.05 ± 1.87%; rTg4510: 53.48 ± 3.24%; rTg21221: 40.25 ± 3.64%. $F(2,19)=42.94$, $P=8.94\times10^{-8}$. All post hoc multiple comparisons between genotypes were significant: $P=5.55\times10^{-8}$ for controls vs. rTg4510, $P=7.85\times10^{-5}$ for controls vs. rTg21221, $P=0.0179$ for rTg4510 vs. rTg21221. The data for the controls and rTg4510 mice are the same as in Fig. 1. Each solid circle represents an individual animal and all error bars reflect the mean ± s.e.m; the differences between genotypes were assessed by one-way ANOVA followed by Tukey's multiple comparisons test, $^{*}P<0.05$, $^{**}P<0.01$, $^{****}P<0.0001$.

APP/PS1-rTg21221 ($n=5$; mean age 7.9 months) mice, but there was also a strong reduction in cortical activity levels (Fig. 3d–j; LMEM for log rates on genetic background, $F(3,5558)=671$, $P=0$; post hoc multiple comparisons between genotypes were all $P<2\times10^{-20}$). Further analysis revealed that, similar to rTg4510 and rTg21221 mice, abnormally silent neurons constitute a large pool of layer 2/3 neurons both in APP/PS1-rTg4510 and APP/PS1-rTg21221 mice (Fig. 3k). We independently obtained similar results in a 17–24-month-old cohort of mice (mean age 20.6 months; Supplementary Fig. 7; see also Supplementary Figs. 2b and 8 for more details on age distributions and the rationale for pooling neuronal data from mice at this 17–24-month age range).

Given that the rTg4510 transgene is associated with an age-dependent loss of neurons, which is enhanced in the APP/PS1-rTg4510 crosses[11], potentially contributing to the observed functional impairments, we next analyzed young, 3–4-month-old rTg4510 mice with and without the APP/PS1 transgene. This analysis revealed a strong reduction in neuronal activities (significant effect of group: $F(3,5594)=14.9$, $P=1.1\times10^{-9}$; post hoc analysis revealed significant differences between the APP/PS1-rTg4510 and all other groups) and increased fractions of silent layer 2/3 neurons in the APP/PS1-rTg4510 crosses already at this early disease stage, before overt neuropathology and neurodegeneration (Supplementary Fig. 9). Supplementary Fig. 10 shows a comparison of the age-dependent changes of cortical neuronal activities for all genotypes. Together, these results indicate that tau blocks Aβ-dependent hyperactivity, resulting in a profound silencing of circuits when both Aβ and tau are present together in the cortex,

and they reinforce the idea that NFTs are not critical for this suppression of neuronal activity.

In the presence of Aβ, tau reduction is less effective in rescuing neuronal impairments. Finally, we employed repeated two-photon Ca^{2+} imaging and determined, in the same mice, whether impaired neuronal circuit function could be rescued by suppressing tau transgene expression. In these experiments, we took advantage of the fact that the tau mice used in this study were equipped with a regulatable promoter system, which allowed us to turn off the expression of the tau transgene by administering a doxycycline (DOX)-containing diet, as demonstrated in several previous studies[22–24]. We carried out two-photon Ca^{2+} imaging of layer 2/3 neurons in the same mice before and six weeks after DOX treatment (all mice were at least six months of age when DOX treatment was started). We found that the neuronal impairments were apparently completely reversed in rTg21221 ($n=8$) and rTg4510 ($n=7$) mice (Fig. 4a–e; Supplementary Fig. 11), despite the continued presence of cortical NFTs (Supplementary Fig. 12a–c). However, instead of the expected rescue of circuit impairment, in all five recorded APP/PS1-rTg4510 and all five recorded APP/PS1-rTg21221 mice there was no apparent change in the fractions of silent neurons after DOX treatment (Fig. 4b–h; Supplementary Fig. 11). The activity levels (Fig. 4c,d,f,g) showed a significant interaction between crossing with APP/PS1 and DOX treatment for both rTg4510 and rTg21221 mice (LMEM for log rates on APP/PS1 crossing and DOX treatment, rTg4510: interaction $F(1,4615)=49.0$, $P=2.8\times10^{-12}$; post hoc, DOX treatment increased significantly ($P<0.05$) the activity level for both crossed and uncrossed strains, but the increase in activity levels for the crossed strain was significantly smaller—compare with Fig. 4c,f; rTg21221: interaction $F(1,3170)=94$, $P=6.1\times10^{-22}$; post hoc, DOX treatment significantly increased activity levels in the uncrossed, but not in the crossed, strain—compare with Fig. 4d,g). Importantly, the observation that tau suppression in the presence of Aβ was significantly less effective in restoring normal neuronal activities could not be explained by the degree of tau reduction, because enzyme-linked immunosorbent assay (ELISA) analysis showed significant and comparable reductions of total human tau levels on DOX treatment in all genotypes (Supplementary Fig. 12d–g). In line with previous reports[22], we also found that sarkosyl-soluble tau levels, measured in forebrain homogenates of rTg4510 mice with and without the APP/PS1 transgene using western blot, were reduced by DOX treatment, while sarkosyl-insoluble fractions were not significantly affected (Supplementary Fig. 13).

To determine if tau suppression would be effective in mice harboring tau and Aβ at an earlier age, before substantial neuropathology and neurodegeneration, we treated 3–4-month-old rTg4510 mice with and without the APP/PS1 transgene with DOX for six weeks. Supplementary Fig. 14 shows that, while there was a significant reduction in the fractions of silent neurons in rTg4510 mice (significant effect of treatment, $F(1,1388)=28.1$, $P=1.3\times10^{-7}$), in APP/PS1-rTg4510 crosses the fractions of silent neurons remained unchanged (no significant effect of treatment, $F(1,3195)=0.47$, $P=0.49$). To show that the effects differed in the rTg4510 mice with and without the APP/PS1 transgene, we performed a LMEM. As expected, there were main effects of APP/PS1 crossing ($F(1,4583)=37.1$, $P=1.2\times10^{-9}$) and of DOX treatment ($F(1,4583)=29.0$, $P=7.4\times10^{-8}$); importantly, the interaction was significant ($F(1,4583)=21.9$, $P=2.9\times10^{-6}$), demonstrating that the difference between the effects of DOX treatment in the young rTg4510 and APP/PS1-rTg4510 mice were highly significant. Again, ELISA analysis showed a substantial reduction in total human tau levels in all mice receiving DOX (Supplementary Fig. 14e,f). As a control, we treated wild-type control mice with DOX and found no significant effects (Supplementary Fig. 15; $F(1,2686)=0.589$, $P=0.44$).

Discussion

Our study reveals that the two major proteins involved in Alzheimer's disease have dramatically opposing effects on the activity of neuronal circuits in vivo. Aβ alone causes hyperactivity, whereas tau alone suppresses activity and promotes silencing of many neurons. Remarkably, neuronal silencing dominates over hyperactivity when Aβ and tau are present together, which is corroborated by a recent in vitro study employing extracellular field recordings in entorhinal cortex slices[25]. However, the dramatic dominance of tau was unexpected in light of previous studies suggesting that tau regulates, and is essential for, Aβ-dependent hyperexcitability[26–28]. While the effects of transgene insertion must always be considered, the Aβ-induced hyperactivity phenotype is observed in multiple amyloid precursor protein (APP)-overexpressing lines with different transgene arrays[29] and is blocked by β-site amyloid precursor protein cleaving enzyme (BACE) inhibitors, which presumably impact primarily Aβ generation[20]; the tau phenotype is observed in two different tau transgenic lines that express two different tau transgenes (tau^{P301L} or wild-type) with substantially different age-related histopathological phenotypes (aggregated tau and NFTs and neurodegeneration in rTg4510, or not in the rTg21221 line). Taken together with the observation that DOX suppression of the transgene ameliorates the abnormal physiology, we believe that the most parsimonious explanation for these observations is that Aβ and tau are responsible for the hyperactivity and suppressed baseline excitability observed in our study.

Our results fit well with and provide a possible cellular explanation for the clinical observations that (1) Alzheimer's disease

Fig. 3 | No hyperactivity and many silent neurons in mice harboring both tau and Aβ. a–c, Coronal sections showing the coexistence of NFTs (green) and Aβ plaques (red) in the cortex of APP/PS1-rTg4510 mice (**b**), but only plaques in APP/PS1 (**a**) and APP/PS1-rTg21221 (**c**) mice. Immunostaining was repeated independently in multiple animals (APP/PS1, $n=7$; APP/PS1-rTg4510, $n=15$; APP/PS1-rTg21221, $n=13$) with similar results. Scale bars, 100 µm. **d**,**e**, Top: in vivo two-photon fluorescence images of layer 2/3 neurons and corresponding activity maps from APP/PS1-rTg4510 (**d**) and APP/PS1-rTg21221 (**e**) mice. Methoxy-X04-labeled plaques are shown in blue. Bottom: spontaneous Ca^{2+} transients of neurons indicated in the top panel. Scale bars, 20 µm. **f–h**, Frequency distribution of all recorded neurons in APP/PS1 (**f**, $n=878$ neurons in 5 mice), APP/PS1-rTg4510 (**g**, $n=2{,}092$ neurons in 8 mice) and APP/PS1-rTg21221 mice (**h**, $n=1{,}050$ neurons in 5 mice). **i**, Summary graph representing the mean frequencies. APP/PS1: 3.42 ± 0.20 transients per min; APP/PS1-rTg4510: 0.52 ± 0.09 transients per min; APP/PS1-rTg21221: 1.16 ± 0.14 transients per min. $F(2,15)=119.9$, $P=5.96\times10^{-10}$. All post hoc multiple comparisons between genotypes were significant: $P=4.36\times10^{-10}$ for APP/PS1 vs. APP/PS1-rTg4510; $P=5.64\times10^{-8}$ for APP/PS1 vs. APP/PS1-rTg21221; $P=0.012$ for APP/PS1-rTg4510 vs. APP/PS1-rTg21221. **j**, Fractions of hyperactive neurons. APP/PS1: $19.11\pm1.50\%$; APP/PS1-rTg4510: $1.00\pm0.43\%$; APP/PS1-rTg21221: $4.25\pm1.13\%$. $F(2,15)=98.35$, $P=2.39\times10^{-9}$. Post hoc multiple comparisons were highly significant: $P=2.02\times10^{-9}$ for APP/PS1 vs. APP/PS1-rTg4510 as well as APP/PS1 vs. APP/PS1-rTg21221 ($P=1.21\times10^{-7}$), but not significant ($P=0.065$) for APP/PS1-rTg4510 vs. APP/PS1-rTg21221. **k**, Fractions of silent neurons. APP/PS1: $9.20\pm2.36\%$; APP/PS1-rTg4510: $62.61\pm2.56\%$; APP/PS1-rTg21221: $44.47\pm4.10\%$. $F(2,15)=80.86$, $P=9.25\times10^{-9}$. All post hoc multiple comparisons between genotypes were significant: $P=5.72\times10^{-9}$ for APP/PS1 vs. APP/PS1-rTg4510; $P=4.87\times10^{-6}$ for APP/PS1 vs. APP/PS1-rTg21221; and $P=0.002$ for APP/PS1-rTg4510 vs. APP/PS1-rTg21221. Data for APP/PS1 mice are the same as shown in Fig. 1. Each solid circle represents an individual animal and all error bars reflect the mean ± s.e.m; the differences among genotypes were assessed by one-way ANOVA followed by Tukey's multiple comparisons test, $^{*}P<0.05$, $^{**}P<0.01$, $^{****}P<0.0001$. NS, not significant.

patients exhibit a progressive decrease of whole-brain activity[30–32] and regional cerebral blood flow[33] as well as a slowing of the electroencephalogram[34], and that (2) tau, rather than Aβ, determines cognitive status[7,35,36]. The dominance of tau could also explain the relative lack of clinical improvement after Aβ suppression in recent clinical trials. In this context, it is noteworthy that Alzheimer's disease carries an increased risk of epileptic seizures[37], and that several studies have shown increased activation of brain regions, such as the hippocampus, using blood oxygenation level-dependent functional magnetic resonance imaging[38,39] (but see Khan et al.[40]). To reconcile these observations with our results, it is important to better understand the precise relationship between single-neuron and (abnormal) population activity. Nonetheless, as neuronal hyperactivity appears to be more related to Aβ[29], it is possible that epileptiform

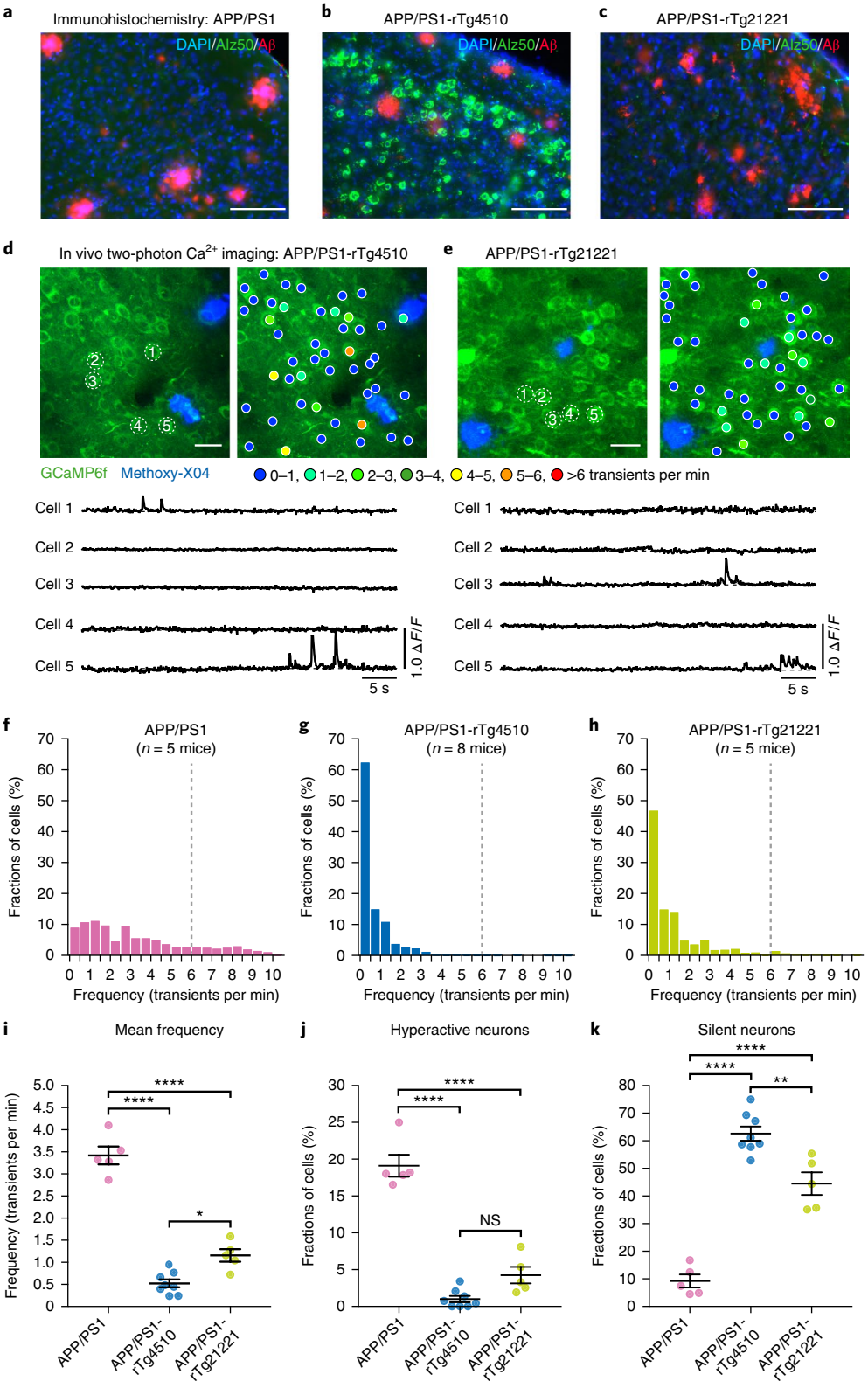

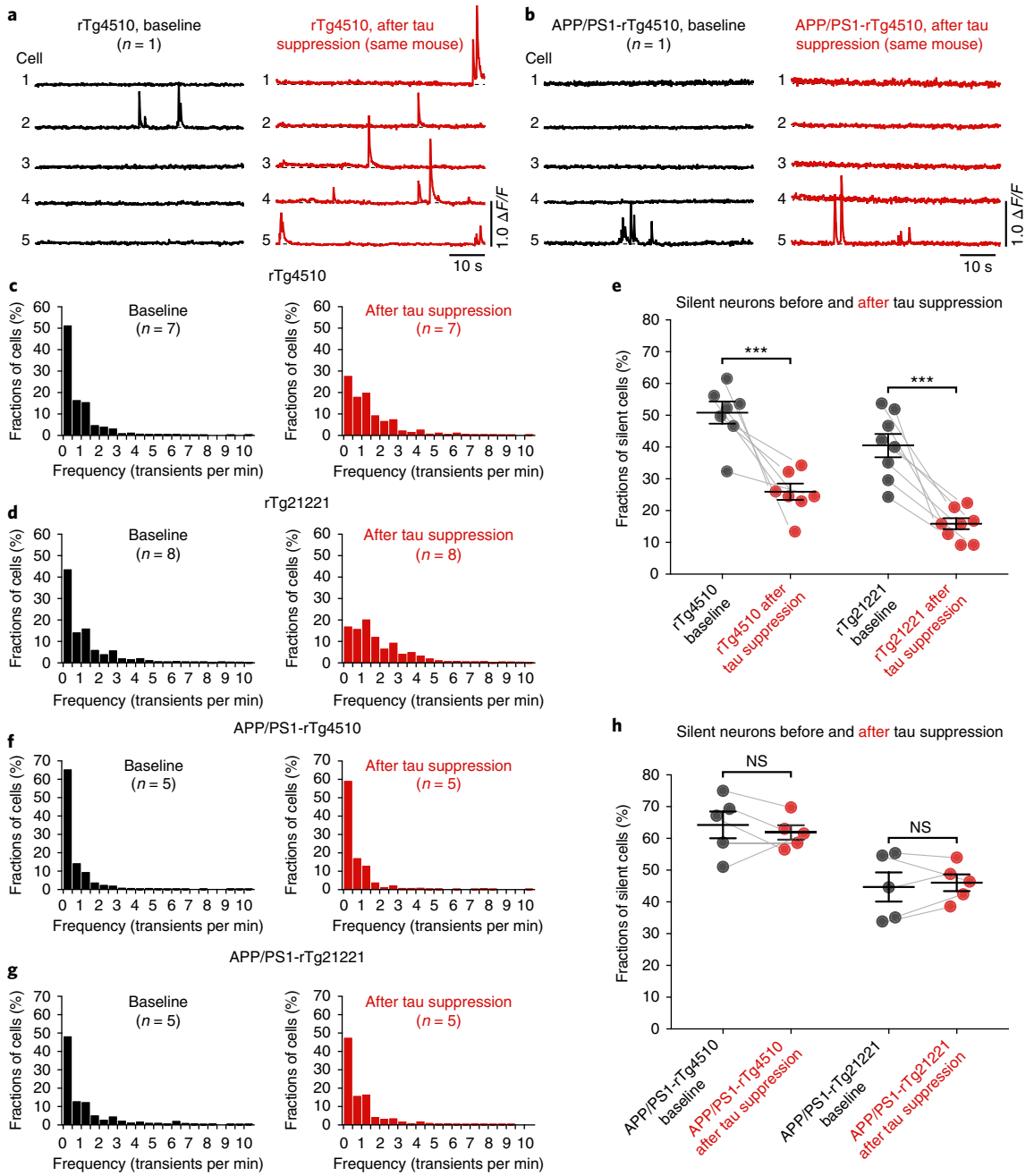

Fig. 4 | Tau transgene suppression rescues neuronal silencing in tau mice but not in mice with tau and Aβ. a,**b**, Example activity traces from neurons before (black) and after (red) tau suppression with DOX in the same rTg4510 (**a**) and APP/PS1-rTg4510 (**b**) mice. **c**,**d**, Frequency distributions of all recorded neurons from rTg4510 mice (**c**) before (baseline, $n = 1{,}412$ neurons in 7 mice) and after ($n = 1{,}118$ neurons in same 7 mice) DOX. The same is shown for rTg21221 mice (**d**) (before DOX, $n = 1{,}675$ neurons in 8 mice; after DOX, $n = 1{,}036$ neurons in same 8 mice). **e**, Fractions of silent neurons in rTg4510 (left; $n = 7$ mice) and rTg21221 (right; $n = 8$ mice) before and after DOX (rTg4510 before DOX, $50.84 \pm 3.49\%$ vs. after DOX, $25.92 \pm 2.57\%$, $t = 5.753$, d.f. $= 11.03$, $P = 1.26 \times 10^{-4}$; rTg21221 before DOX, $40.45 \pm 3.68\%$ vs. after DOX, $15.87 \pm 1.74\%$, $t = 6.047$, d.f. $= 9.972$, $P = 1.26 \times 10^{-4}$). **f**, Frequency distributions from APP/PS1-rTg4510 mice before ($n = 1{,}262$ neurons in 5 mice) and after ($n = 827$ neurons in same 5 mice) DOX. **g**, The same is shown for APP/PS1-rTg21221 mice (before DOX, $n = 795$ neurons in 5 mice; after DOX, $n = 904$ neurons in the same 5 mice). **h**, Fractions of silent neurons in APP/PS1-rTg4510 (left; $n = 5$ mice) and APP/PS1-rTg21221 (right; $n = 5$ mice) before and after DOX. APP/PS1-rTg4510 before DOX, $64.25 \pm 4.21\%$ vs. after DOX, $61.87 \pm 2.28\%$, $t = 0.4962$, d.f. $= 6.152$, $P = 0.6370$. APP/PS1-rTg21221 before DOX, $44.72 \pm 4.59\%$ versus after DOX, $46.04 \pm 2.64\%$, $t = 0.2494$, d.f. $= 6.387$, $P = 0.8109$. Each solid circle represents an individual animal and the error bars represent the mean ± s.e.m.; the differences among groups were assessed using two-sided Welch's t tests, $^{***}P < 0.001$. NS, not significant.

activity and blood oxygenation level-dependent hyperactivation are more prominent in Alzheimer's disease patients who have relatively higher Aβ than tau levels, that is, at very early (possibly presymptomatic) points in the disease process when Aβ deposits occur throughout the cortex, but NFTs are limited to the medial temporal lobe. This appears to be the case for hyperactivity in the hippocampus diagnosed with functional magnetic resonance imaging[38]. Our finding that tau suppresses neuronal activity agrees with previous electrophysiological studies[41–43] and goes on to demonstrate that soluble, non-aggregated tau is sufficient for neuronal silencing, and

that NFTs are not required. The link between soluble tau and neuronal dysfunction may provide a mechanistic explanation for the observation that, in mouse models, cognitive deficits occur independently of NFT formation[22,44–48]; that NFTs are not necessarily associated with functional impairments is also in line with previous studies showing that NFT-bearing cortical neurons can reliably respond to strong synaptic inputs, for example, during simple sensory stimuli[49,50]. Another unexpected but intriguing result of our study was the finding that suppression of tau gene expression rescued neuronal circuit impairments in tau mice, but was significantly less effective when Aβ was present at the same time. This lack of effect was present already in young mice, before substantial neuropathology, synapse loss, and neurodegeneration; nonetheless, it may be related to more severe and persisting synaptic and cellular changes in the context of (soluble) Aβ-tau interactions compared to Aβ or tau alone. Notably, aggregated tau in NFTs is the target for several ongoing clinical trials; our current data argue that readouts for these trials also need to be reconsidered. Together, our results clarify the pathological role of interaction between Aβ and tau in impairing neuronal circuit integrity and function in Alzheimer's disease, with important mechanistic and therapeutic implications not only for Alzheimer's disease, but also for other tauopathies and conditions that are associated with elevated tau.

Online content

Any methods, additional references, Nature Research reporting summaries, source data, statements of data availability and associated accession codes are available at https://doi.org/10.1038/s41593-018-0289-8.

Received: 24 August 2018; Accepted: 9 November 2018;
Published online: 17 December 2018

References

1. Hyman, B. T. et al. National Institute on Aging-Alzheimer's Association guidelines for the neuropathologic assessment of Alzheimer's disease. *Alzheimers Dement.* **8**, 1–13 (2012).
2. Braak, H. & Braak, E. Neuropathological stageing of Alzheimer-related changes. *Acta Neuropathol.* **82**, 239–259 (1991).
3. Arnold, S. E., Hyman, B. T., Flory, J., Damasio, A. R. & Van Hoesen, G. W. The topographical and neuroanatomical distribution of neurofibrillary tangles and neuritic plaques in the cerebral cortex of patients with Alzheimer's disease. *Cereb. Cortex* **1**, 103–116 (1991).
4. Schöll, M. et al. PET imaging of tau deposition in the aging human brain. *Neuron* **89**, 971–982 (2016).
5. Delacourte, A. et al. The biochemical pathway of neurofibrillary degeneration in aging and Alzheimer's disease. *Neurology* **52**, 1158–1165 (1999).
6. Wang, L. et al. Evaluation of tau imaging in staging Alzheimer disease and revealing interactions between β-amyloid and tauopathy. *JAMA Neurol.* **73**, 1070–1077 (2016).
7. Pontecorvo, M. J. et al. Relationships between flortaucipir PET tau binding and amyloid burden, clinical diagnosis, age and cognition. *Brain* **140**, 748–763 (2017).
8. Lewis, J. et al. Enhanced neurofibrillary degeneration in transgenic mice expressing mutant tau and APP. *Science* **293**, 1487–1491 (2001).
9. Götz, J., Chen, F., van Dorpe, J. & Nitsch, R. M. Formation of neurofibrillary tangles in P301l tau transgenic mice induced by $A\beta_{42}$ fibrils. *Science* **293**, 1491–1495 (2001).
10. Hurtado, D. E. et al. Aβ accelerates the spatiotemporal progression of tau pathology and augments tau amyloidosis in an Alzheimer mouse model. *Am. J. Pathol.* **177**, 1977–1988 (2010).
11. Bennett, R. E. et al. Enhanced tau aggregation in the presence of amyloid β. *Am. J. Pathol.* **187**, 1601–1612 (2017).
12. Jacobs, H. I. L. et al. Structural tract alterations predict downstream tau accumulation in amyloid-positive older individuals. *Nat. Neurosci.* **21**, 424–431 (2018).
13. Quiroz, Y. T. et al. Association between amyloid and tau accumulation in young adults with autosomal dominant Alzheimer disease. *JAMA Neurol.* **75**, 548–556 (2018).
14. He, Z. et al. Amyloid-β plaques enhance Alzheimer's brain tau-seeded pathologies by facilitating neuritic plaque tau aggregation. *Nat. Med.* **24**, 29–38 (2018).
15. Kerr, J. N., Greenberg, D. & Helmchen, F. Imaging input and output of neocortical networks in vivo. *Proc. Natl. Acad. Sci. USA* **102**, 14063–14068 (2005).
16. Chen, T. W. et al. Ultrasensitive fluorescent proteins for imaging neuronal activity. *Nature* **499**, 295–300 (2013).
17. Busche, M. A. et al. Clusters of hyperactive neurons near amyloid plaques in a mouse model of Alzheimer's disease. *Science* **321**, 1686–1689 (2008).
18. Grienberger, C. et al. Staged decline of neuronal function in vivo in an animal model of Alzheimer's disease. *Nat. Commun.* **3**, 774 (2012).
19. Busche, M. A. et al. Decreased amyloid-β and increased neuronal hyperactivity by immunotherapy in Alzheimer's models. *Nat. Neurosci.* **18**, 1725–1727 (2015).
20. Keskin, A. D. et al. BACE inhibition-dependent repair of Alzheimer's pathophysiology. *Proc. Natl. Acad. Sci. USA* **114**, 8631–8636 (2017).
21. Jackson, R. J. et al. Human tau increases amyloid β plaque size but not amyloid β-mediated synapse loss in a novel mouse model of Alzheimer's disease. *Eur. J. Neurosci.* **44**, 3056–3066 (2016).
22. Santacruz, K. et al. Tau suppression in a neurodegenerative mouse model improves memory function. *Science* **309**, 476–481 (2005).
23. Berger, Z. et al. Accumulation of pathological tau species and memory loss in a conditional model of tauopathy. *J. Neurosci.* **27**, 3650–3662 (2007).
24. de Calignon, A. et al. Caspase activation precedes and leads to tangles. *Nature* **464**, 1201–1204 (2010).
25. Angulo, S. L. et al. Tau and amyloid-related pathologies in the entorhinal cortex have divergent effects in the hippocampal circuit. *Neurobiol. Dis.* **108**, 261–276 (2017).
26. Roberson, E. D. et al. Reducing endogenous tau ameliorates amyloid β-induced deficits in an Alzheimer's disease mouse model. *Science* **316**, 750–754 (2007).
27. Ittner, L. M. et al. Dendritic function of tau mediates amyloid-β toxicity in Alzheimer's disease mouse models. *Cell* **142**, 387–397 (2010).
28. DeVos, S. L. et al. Antisense reduction of tau in adult mice protects against seizures. *J. Neurosci.* **33**, 12887–12897 (2013).
29. Zott, B., Busche, M. A., Sperling, R. A. & Konnerth, A. What happens with the circuit in Alzheimer's disease in mice and humans? *Annu. Rev. Neurosci.* **41**, 277–297 (2018).
30. Silverman, D. H. et al. Positron emission tomography in evaluation of dementia: regional brain metabolism and long-term outcome. *JAMA* **286**, 2120–2127 (2001).
31. Alexander, G. E., Chen, K., Pietrini, P., Rapoport, S. I. & Reiman, E. M. Longitudinal PET evaluation of cerebral metabolic decline in dementia: a potential outcome measure in Alzheimer's disease treatment studies. *Am. J. Psychiatry* **159**, 738–745 (2002).
32. Greicius, M. D., Srivastava, G., Reiss, A. L. & Menon, V. et al. Default-mode network activity distinguishes Alzheimer's disease from healthy aging: evidence from functional MRI. *Proc. Natl. Acad. Sci. USA* **101**, 4637–4642 (2004).
33. Bradley, K. M. et al. Cerebral perfusion SPET correlated with Braak pathological stage in Alzheimer's disease. *Brain* **125**, 1772–1781 (2002).
34. Jelic, V. et al. Apolipoprotein E epsilon4 allele decreases functional connectivity in Alzheimer's disease as measured by EEG coherence. *J. Neurol. Neurosurg. Psychiatry* **63**, 59–65 (1997).
35. Arriagada, P. V., Growdon, J. H., Hedley-Whyte, E. T. & Hyman, B. T. Neurofibrillary tangles but not senile plaques parallel duration and severity of Alzheimer's disease. *Neurology* **42**, 631–639 (1992).
36. Nelson, P. T. et al. Correlation of Alzheimer disease neuropathologic changes with cognitive status: a review of the literature. *J. Neuropathol. Exp. Neurol.* **71**, 362–381 (2012).
37. Palop, J. J. & Mucke, L. Network abnormalities and interneuron dysfunction in Alzheimer disease. *Nat. Rev. Neurosci.* **17**, 777–792 (2016).
38. Dickerson, B. C. et al. Increased hippocampal activation in mild cognitive impairment compared to normal aging and AD. *Neurology* **65**, 404–411 (2005).
39. Bakker, A. et al. Reduction of hippocampal hyperactivity improves cognition in amnestic mild cognitive impairment. *Neuron* **74**, 467–474 (2012).
40. Khan, U. A. et al. Molecular drivers and cortical spread of lateral entorhinal cortex dysfunction in preclinical Alzheimer's disease. *Nat. Neurosci.* **17**, 304–311 (2014).
41. Hoover, B. R. et al. Tau mislocalization to dendritic spines mediates synaptic dysfunction independently of neurodegeneration. *Neuron* **68**, 1067–1081 (2010).
42. Menkes-Caspi, N. et al. Pathological tau disrupts ongoing network activity. *Neuron* **85**, 959–966 (2015).
43. Hatch, R. J., Wei, Y., Xia, D. & Götz, J. Hyperphosphorylated tau causes reduced hippocampal CA1 excitability by relocating the axon initial segment. *Acta Neuropathol.* **133**, 717–730 (2017).
44. Oddo, S. et al. Reduction of soluble Aβ and tau, but not soluble Aβ alone, ameliorates cognitive decline in transgenic mice with plaques and tangles. *J. Biol. Chem.* **281**, 39413–39423 (2006).

45. Sydow, A. et al. Tau-induced defects in synaptic plasticity, learning, and memory are reversible in transgenic mice after switching off the toxic Tau mutant. *J. Neurosci.* **31**, 2511–2525 (2011).
46. Lasagna-Reeves, C. A. et al. Tau oligomers impair memory and induce synaptic and mitochondrial dysfunction in wild-type mice. *Mol. Neurodegener.* **6**, 39 (2011).
47. Van der Jeugd, A. et al. Cognitive defects are reversible in inducible mice expressing pro-aggregant full-length human Tau. *Acta Neuropathol.* **123**, 787–805 (2012).
48. Castillo-Carranza, D. L. et al. Passive immunization with Tau oligomer monoclonal antibody reverses tauopathy phenotypes without affecting hyperphosphorylated neurofibrillary tangles. *J. Neurosci.* **34**, 4260–4272 (2014).
49. Rudinskiy, N. et al. Tau pathology does not affect experience-driven single-neuron and network-wide Arc/Arg3.1 responses. *Acta Neuropathol. Commun.* **2**, 63 (2014).
50. Kuchibhotla, K. V. et al. Neurofibrillary tangle-bearing neurons are functionally integrated in cortical circuits in vivo. *Proc. Natl. Acad. Sci. USA* **111**, 510–514 (2014).

Acknowledgements

We thank A.B. Robbins, D.L. Corjuc, A.D. Roe, and E. Hudry for their excellent technical support, and all members of the Hyman laboratory for providing comments and advice throughout the project. We thank Matthias Staufenbiel for helpful discussions and experimental suggestions. We acknowledge the Genetically-Encoded Neuronal Indicator and Effector (GENIE) project and the Janelia Research Campus of the Howard Hughes Medical Institute and specifically V. Jayaraman, R.A. Kerr, D.S. Kim, L.L. Looger, and K. Svoboda from the GENIE Project, Janelia Research Campus, Howard Hughes Medical Institute for making AAV.Syn.GCaMP6f publicly available. We thank Dr P. Davies for kindly providing the PHF1 and Alz50 antibodies. We thank the following funding agencies for their support: M.A.B. was supported by an EMBO Long-Term Fellowship (grant no. ALTF 590-2016), the Alzheimer Forschung Initiative, and the UK Dementia Research Institute. I.N. was supported by an advanced ERC grant (project RATLAND; grant no. 340063). B.T.H. received support from the Massachusetts Alzheimer's Disease Research Center (grant no. P50AG005134), the JPB foundation, the National Institutes of Health (grant no. 1R01AG0586741), and the Tau Consortium.

Author contributions

M.A.B. and B.T.H. designed the study. M.A.B., S.W., S.D., C.C., J.S., N.K., and T.V.K. performed the research. M.A.B., S.W., S.D., C.C., and I.N. analyzed the data. G.A.C. provided the background information regarding mouse breeding. M.A.B. and B.T.H. wrote the manuscript with input from all other authors.

Competing interests

The authors declare no competing interests.

Additional information

Supplementary information is available for this paper at https://doi.org/10.1038/s41593-018-0289-8.

Reprints and permissions information is available at www.nature.com/reprints.

Correspondence and requests for materials should be addressed to M.A.B. or B.T.H.

Publisher's note: Springer Nature remains neutral with regard to jurisdictional claims in published maps and institutional affiliations.

© The Author(s), under exclusive licence to Springer Nature America, Inc. 2018

Methods

Animals. The generation, care, and use of animals as well as all experimental procedures were approved by the Institutional Animal Care and Use Committees of the Massachusetts General Hospital and McLaughlin Research Institute for Biomedical Sciences. All mice were housed in standard mouse cages on wood bedding under conventional laboratory conditions (12-h dark and 12-h light cycle, constant temperature and humidity); they were given food and water ad libitum. Male and female mice were used in the study and randomly allocated to the experiments. B6.Cg-Tg(APPswe, PSEN1dE9)85Dbo/MmJ mice (henceforth designated APP/PS1) were initially obtained from The Jackson Laboratory[51]. APP/PS1 mice were crossed with the B6.Cg-Tg(Camk2a-tTA)1/Mmay tet transactivator strain that expresses tetracycline-controlled transactivator protein (tTA) from the CK-tTA transgene exclusively in the forebrain[52]. Double transgenic B6.CK-tTA, APP/PS1 males were selected as sires for the experimental cross with dams from the tetracycline-responsive element strain FVB-Tg(tetO-MAPT*P301L)4510/Kha/Jlws (henceforth Tg4510) or FVB-Tg(tetO-MAPT*wt)21221 (henceforth Tg21221) to produce APP/PS1-rTg4510 or APP/PS1-rTg21221 mice with the experimental, tau-expressing genotypes plus mice negative for either the responder or transactivator transgene that do not express any human tau. All of the same sex offspring of these crosses share the FVBB6F1 background and are genetically identical to one another except for the transgene arrays that they carry.

Surgery and injection of genetically encoded Ca^{2+} indicator. Mice were initially anesthetized with 4% isoflurane in O_2 and maintained on 2% isoflurane during the surgical procedure. The body temperature of the anesthetized mice was maintained at ~37.5 °C using a heating pad; ophthalmic ointment was applied to protect the eyes. Using aseptic techniques, the skin above the skull was removed and, by using a fine-tipped dental drill, two craniotomies were performed over the left and right parietal cortices. Then, the fast and ultrasensitive genetically encoded fluorescent Ca^{2+} sensor GCaMP6f[16] (AAV1.Syn.GCaMP6f.WPRE.SV40; purchased from University of Pennsylvania Vector Core), was stereotactically (Kopf Instruments) injected into layer 2/3 (~300 µm deep) at a rate of 0.2 µl min^{-1} using a Pump 11 Elite microsyringe pump (Harvard Apparatus). A single injection (~1 µl of viral construct) was made in each cortical hemisphere. A round glass coverslip (8 mm diameter) was placed over both craniotomies and sealed to the bone using a mix of dental cement and cyanoacrylate[50]. After surgery, mice were returned to their home cage for 2–3 weeks. Analgesia (buprenorphine and acetaminophen) was continued for 3 d postoperatively.

In vivo two-photon fluorescence microscopy. To minimize brain state-dependent experimental variables[53] and for better comparison with previous studies[17–20], in the present study imaging was performed under light isoflurane anesthesia. Mice were anesthetized with 4% isoflurane in O_2 for induction; a reduced concentration of isoflurane (~1%) was used during the imaging. After induction, we waited at least 60 min before imaging. The animal's body temperature was maintained at ~37.5 °C with a heating pad; ophthalmic ointment was applied to protect the eyes. Two-photon imaging was performed on a Fluoview FV1000MPE multiphoton microscope (Olympus) equipped with a mode-locked MaiTai Ti:sapphire laser (Spectra-Physics) tuned to 900 nm. Spontaneous Ca^{2+} fluorescence signals from cortical layer 2/3 were recorded at ~15 Hz through a 25×, 1.05 numerical aperture water immersion objective (6× digital zoom; Olympus). Scanning and image acquisition was controlled by the Fluoview software (Olympus). Imaging was carried out across multiple fields of view (256 × 256 pixels, 84.41 × 84.41 µm) per mouse, and each field of view was recorded for at least 130 s. Image analysis was performed offline using the Fiji package of ImageJ (National Institutes of Health) and Igor Pro (WaveMetrics). First, regions of interest were drawn around individual neuronal somata; then, relative GCaMP6f fluorescence change versus time traces were generated for each region of interest. Ca^{2+} transients were identified as changes in relative fluorescence that were three times larger than the s.d. of the baseline fluorescence. Based on previous protocols[19,20], neurons were classified according to their individual activity rates as silent (0 transients per min), normal (0–6 transients per min), or hyperactive (≥6 transients per min).

Immunohistochemistry. Brain hemispheres from mice were drop fixed in 4% paraformaldehyde in PBS for 48 h at 4 °C. After fixation, brains were washed with PBS, cryoprotected with 30% sucrose, and sliced into 40-µm-thick coronal sections with a sliding microtome (SM2000 R; Leica). Sections were rinsed three times in Tris-buffered saline (TBS) and then permeabilized with 0.2% Triton X-100 in TBS for 20 min. Sections were then blocked in 10% normal goat serum (NGS) in TBS for 60 min at room temperature, followed by overnight incubation at 4 °C in primary antibodies diluted in 5% NGS. The following primary antibodies were used: mouse anti-Alz50 immunoglobulin M (IgM, 1:500, courtesy of Peter Davies); chicken anti-GFP (1:1,000; Aves Labs); rabbit anti-human Aβ (1:500; IBL America); mouse anti-PHF1 IgG (1:1,000, courtesy of Peter Davies). After three washes in TBS, sections were incubated in secondary antibodies diluted in 5% NGS for 60 min at room temperature. After three washes in TBS, sections were incubated in secondary antibodies diluted in 5% NGS for 60 min at room temperature. The following secondary antibodies were used: goat anti-mouse IgM, µ chain, Cy3 conjugate (1:1,000; EMD Millipore); Alexa Fluor 488 goat anti-chicken (1:1,000; Invitrogen); Alexa Fluor 647 goat anti-rabbit (1:500; Invitrogen); Alexa Fluor 647 goat anti-mouse IgG (1:500; Invitrogen). After three washes in TBS, sections were mounted on microscope slides in 4,6-diamidino-2-phenylindole (DAPI) VECTASHIELD Antifade Mounting Medium (Vector Laboratories) and coverslipped. Images were recorded on a Axio Imager microscope (ZEISS) equipped with a CoolSNAP digital camera (Photometrics) and AxioVision software version 4.8. Stereological quantifications of NFTs and amyloid plaques were performed using the Computer Assisted Stereological Toolbox (Olympus). All counting was conducted blinded to genotype and treatment. Further information about the antibodies used for immunohistochemistry can be found in the Life Sciences Reporting Summary.

Tau protein analysis. Mouse forebrain was homogenized with a dounce homogenizer in 300 µl PBS with protease inhibitor (100:1, Thermo Fisher Scientific) and spun at 10,000*g* for 10 min at 4 °C. The pellet was collected for sarkosyl extraction. Protein concentration was determined with a Pierce BCA Protein Assay Kit (Thermo Fisher Scientific). ELISA was performed using the Phospho(Thr231)/Total Tau Kit (MSD), following the manufacturer's protocol. All samples were run in duplicate and fitted to an eight-point standard curve to determine concentration. To isolate sarkosyl-soluble/insoluble tau, the same protein quantity of mouse brain lysate pellet was resuspended in cold TBS and centrifuged at 150,000*g* for 15 min at 4 °C. The pellet was then homogenized in 3× salt/sucrose buffer (0.8 M NaCl, 10% sucrose, 10 mN Tris base, pH 7.4) and centrifuged at 150,000*g* for 15 min at 4 °C. The supernatant was collected, adjusted to 1% sarkosyl and incubated for 1 h at 37 °C. Samples were then centrifuged at 150,000*g* for 30 min at 4 °C. The supernatant and pellets were collected. Pellets were resuspended with radioimmunoprecipitation assay buffer containing 1% SDS and sonicated for 20 min in a Branson 2510 sonicator. Both supernatant (sarkosyl-soluble) and pellets (sarkosyl-insoluble) were then analyzed by western blot as follows: sarkosyl-soluble and insoluble fractions were mixed with 1× final lithium dodecyl sulfate sample buffer (Invitrogen) and 50 mM dithiothreitol (10× Sample Reducing Agent; Invitrogen), and boiled for 5 min. Samples were loaded in 4–12% Bis-Tris gel (Invitrogen) and run at 130 V for 90 min in 1× MES SDS Running Buffer (Invitrogen). Proteins were then transferred to an activated polyvinylidene fluoride membrane (EMD Millipore) in 1× transfer buffer (Bio-Rad Laboratories) at 75 V for 75 min. Membranes were then blocked for 1 h using the Odyssey Blocking Buffer (LI-COR Biosciences) at room temperature and then incubated with a mouse anti-human Tau antibody (TAU-13, 1:2,500; BioLegend) and a chicken anti-glyceraldehyde 3-phosphate dehydrogenase antibody (1:5,000; EMD Millipore) in blocking buffer (LI-COR Biosciences) overnight at 4 °C. Membranes were then washed 3 × 10 min in TBS with Tween 20, and then incubated with secondary antibodies (goat anti-mouse IgG IRDye 680RD and donkey anti-chicken IgG IRDye 800CW; both LI-COR Biosciences) for 1 h at room temperature. Membranes were imaged using a LI-COR Biosciences imaging station using the Odyssey software. Blots were converted to gray scale and densitometry analysis was performed in ImageJ. Further information about the antibodies used for tau protein analysis can be found in the Life Sciences Reporting Summary.

Statistics. No statistical methods were used to predetermine sample sizes; however, our sample sizes are similar to those reported in previous publications (see, for example, Busche et al.[17], Grienberger et al.[18], Busche et al.[19], and Keskin et al.[20]). No animals or data points were excluded from the analysis. Biochemical and histological analyses were conducted blinded to genotype and treatment, whereas in vivo microscopy and analysis were not performed blinded to the conditions of the experiments. The distributions of firing rates of neurons were analyzed using LMEMs with animal as a random factor, and fixed factors as stated in the main text. Since the distributions of firing rates were highly skewed to the right, a log transformation was used to ensure normality. This was the best Box–Cox transformation for these data. Firing rates of 0 were coded as half the lowest non-zero observed rate before the log transformation. Computations were performed using the function fitlme in the statistical toolbox of Matlab version R2017b (MathWorks). Statistical comparison between two experimental groups was assessed with a two-sided Welch's *t* test; differences between multiple groups were assessed using one-way analysis of variance (ANOVA) followed by a Tukey's multiple comparisons test. $P < 0.05$ was considered statistically significant. Analysis routines and the code used in this study can be requested from the corresponding authors.

Reporting Summary. Further information on research design is available in the Nature Research Reporting Summary linked to this article.

Data availability

All data are reported in the main text and supplementary materials, stored at the Massachusetts General Hospital, and are available from the corresponding authors upon reasonable request.

References

51. Jankowsky, J. L. et al. Mutant presenilins specifically elevate the levels of the 42 residue β-amyloid peptide in vivo: evidence for augmentation of a 42-specific gamma secretase. *Hum. Mol. Genet.* **13**, 159–170 (2004).
52. Mayford, M. et al. Control of memory formation through regulated expression of a CaMKII transgene. *Science* **274**, 1678–1683 (1996).
53. Froudarakis, E. et al. Population code in mouse V1 facilitates readout of natural scenes through increased sparseness. *Nat. Neurosci.* **17**, 851–857 (2014).

nature research

Corresponding author(s): Marc Aurel Busche and Bradley T. Hyman

Reporting Summary

Nature Research wishes to improve the reproducibility of the work that we publish. This form provides structure for consistency and transparency in reporting. For further information on Nature Research policies, see Authors & Referees and the Editorial Policy Checklist.

Statistical parameters

When statistical analyses are reported, confirm that the following items are present in the relevant location (e.g. figure legend, table legend, main text, or Methods section).

n/a	Confirmed	
☐	☒	The exact sample size (*n*) for each experimental group/condition, given as a discrete number and unit of measurement
☐	☒	An indication of whether measurements were taken from distinct samples or whether the same sample was measured repeatedly
☐	☒	The statistical test(s) used AND whether they are one- or two-sided *Only common tests should be described solely by name; describe more complex techniques in the Methods section.*
☒	☐	A description of all covariates tested
☒	☐	A description of any assumptions or corrections, such as tests of normality and adjustment for multiple comparisons
☐	☒	A full description of the statistics including central tendency (e.g. means) or other basic estimates (e.g. regression coefficient) AND variation (e.g. standard deviation) or associated estimates of uncertainty (e.g. confidence intervals)
☒	☐	For null hypothesis testing, the test statistic (e.g. *F*, *t*, *r*) with confidence intervals, effect sizes, degrees of freedom and *P* value noted *Give P values as exact values whenever suitable.*
☒	☐	For Bayesian analysis, information on the choice of priors and Markov chain Monte Carlo settings
☐	☒	For hierarchical and complex designs, identification of the appropriate level for tests and full reporting of outcomes
☒	☐	Estimates of effect sizes (e.g. Cohen's *d*, Pearson's *r*), indicating how they were calculated
☐	☒	Clearly defined error bars *State explicitly what error bars represent (e.g. SD, SE, CI)*

Our web collection on statistics for biologists may be useful.

Software and code

Policy information about availability of computer code

Data collection	In vivo image aquisition was controlled by the Fluoview Software FV10-ASW (Olympus, ver. 04.02). Immunhistochemical images were collected with a Zeiss Axio-Imager microscope equipped with a Coolsnap digital camera and Axio-Vision V4.8. Stereological quantifications of tau neurofibrillary tangles and amyloid plaques were performed using the Computer Assisted Stereological Toolbox (Olympus). Western blot membranes were imaged using a LI-COR imaging station equipped with the Odyssey software (ver. 3.0). ELISA analysis was performed using the Meso Scale Diagnostics (MSD) Phospho (Thr231)/Total Human Tau ELISA kit (MSD #K15121D).
Data analysis	Analysis of imaging and Western blot data was performed using the Fiji Package of ImageJ (NIH, ver. 2.0.0-rc-59/1.51k), as well as IGOR Pro (Wavemetrics, ver. 6.32). Graphs were generated in GraphPad Prism 7. Statistical analysis was carried out using GraphPad Prism 7 and MATLAB 2017b.

For manuscripts utilizing custom algorithms or software that are central to the research but not yet described in published literature, software must be made available to editors/reviewers upon request. We strongly encourage code deposition in a community repository (e.g. GitHub). See the Nature Research guidelines for submitting code & software for further information.

Data

Policy information about availability of data

All manuscripts must include a data availability statement. This statement should provide the following information, where applicable:

- Accession codes, unique identifiers, or web links for publicly available datasets
- A list of figures that have associated raw data
- A description of any restrictions on data availability

All data are reported in the main text and supplementary materials, stored at the Massachusetts General Hospital, and available upon reasonable request.

Field-specific reporting

Please select the best fit for your research. If you are not sure, read the appropriate sections before making your selection.

☒ Life sciences ☐ Behavioural & social sciences ☐ Ecological, evolutionary & environmental sciences

For a reference copy of the document with all sections, see nature.com/authors/policies/ReportingSummary-flat.pdf

Life sciences study design

All studies must disclose on these points even when the disclosure is negative.

Sample size	We aimed for high-quality recordings from a commonly used and statistically sufficient sample size. Sample size was chosen on the basis of pilot experiments, previous experiences with similar types of experiments and was similar to those reported in previous publications (see e.g. refs. 17-20). We also found that the variability between individual animals and recordings was low, which indicates that acquisition of additional data would not alter our results.
Data exclusions	No data points were excluded from the analysis.
Replication	All findings in this study were collected from multiple independent experiments, and were reliably reproduced.
Randomization	For all experiments, mice were selected randomly.
Blinding	For all experiments, the experimenter was aware of the conditions being tested. Importantly, all data analysis was performed using semi-automated routines, developed prior to data acquisition. All biochemical analyses and counting of amyloid plaques and tau tangles was conducted blinded to genotype and treatment.

Reporting for specific materials, systems and methods

Materials & experimental systems

n/a	Involved in the study
☒	☐ Unique biological materials
☐	☒ Antibodies
☒	☐ Eukaryotic cell lines
☒	☐ Palaeontology
☐	☒ Animals and other organisms
☒	☐ Human research participants

Methods

n/a	Involved in the study
☒	☐ ChIP-seq
☒	☐ Flow cytometry
☒	☐ MRI-based neuroimaging

Antibodies

Antibodies used	1) Mouse anti-Alz50 IgM (1:500, courtesy of Peter Davies), this antibody is widely used and has been originally validated by Wolozin et al., A neuronal antigen in the brains of Alzheimer patients, Science, 1986. See also: https://www.alzforum.org/antibodies/tau-alz50-0. 2) Mouse anti-PHF1 IgG (1:1000, courtesy of Peter Davies), this antibody is commonly used in the Hyman laboratory as well as by many other labs and has been validated in several previous publications, see e.g. Wegmann et al., Tau protein liquid–liquid phase separation can initiate tau aggregation, EMBO Journal 2018; see also https://www.alzforum.org/antibodies/tau-phos-ser396ser404-phf-1.

3) Tau-13 (1:2500, Biolegend, cat. no. 835201, lot B253430, clone Tau-13), this antibody is widely used and has been validated and used in the Hyman laboratory as well as in multiple previous publications that are listed on the manufacturer's website.

4) Rabbit anti-Human Aβ (1:500, IBL America, cat. no. 18584, lot 1E-330, polyclonal), this antibody has been used and validated in several previous studies including Hudry et al., Gene transfer of human APOE isoforms results in differential modulation of amyloid deposition and neurotoxicity in mouse brain, Sci. Transl. Med., 2013.

5) Chicken anti-GFP (1:1000, Aves Labs, cat. no. GFP-1020, lot 0511FP12, polyclonal), the antibody has been used and validated in previous publications from the Hyman laboratory, see e.g. Hudry et al., Exosome-associated AAV vector as a robust and convenient neuroscience tool, Gene Therapy, 2016.

6) Goat anti-mouse IgM cy3 (1:1000, Millipore, cat. no. AP128C, lot 2978936, polyclonal), this antibody has been validated in previous publications that are listed on the manufacturer's website.

7) Alexa Fluor488 goat anti-chicken (1:1000, Invitrogen, cat. no. A11039, lot 1899514, polyclonal), this antibody has been validated in several previous publications that are listed on the manufacturer's website.

8) Alexa Fluor647 goat anti-rabbit (1:500, Invitrogen, cat. no. A21245, lot 1922848, polyclonal), this antibody has been validated in several previous publications that are listed on the manufacturer's website.

9) Alexa Fluor647 goat anti-mouse IgG (1:500, Invitrogen, cat. no. A21235, lot 1837146, polyclonal), Alexa Fluor647 goat anti-mouse IgG (1:500, Invitrogen, cat. no. A21235, polyclonal), this antibody has been validated in several previous publications that are listed on the manufacturer's website.

10) Chicken anti-GAPDH antibody (1:5000, EMD Millipore Corp, AB2302, lot 3022890, polyclonal), this antibody has been validated and used in the Hyman laboratory and in multiple previous publications that are listed in the manufacturer's website.

Validation

All antibodies have been validated for the applications used within this manuscript (see above) and for the commercial antibodies this information is available on the manufacturers' publicly accessible datasheets. The tau antibodies Alz50, PHF1 and Tau-13 have been extensively used and validated in the Hyman laboratory (including immunohistochemistry in tg4510 and tau null tissue) and have been published previously in multiple studies by many different laboratories.

Animals and other organisms

Policy information about studies involving animals; ARRIVE guidelines recommended for reporting animal research

Laboratory animals

B6.Cg-Tg(APPswe, PSEN1dE9)85Dbo/MmJ mice (hereafter designated APP/PS1) were initially obtained from Jackson Laboratory (Bar Harbor, ME). APP/PS1 mice were crossed to the B6.Cg-Tg(Camk2a-tTA)1/Mmay tet transactivator strain that expresses tTA from the CK-tTA transgene exclusively in the forebrain (see ref. 59). Double transgenic B6.CK-tTA, APP/PS1 males were selected as sires for the experimental cross to dams from the tetracycline-responsive element strain FVB-Tg(tetO-MAPT*P301L)4510/Kha/Jlws (Tg4510) or FVB-Tg(tetO-MAPT*wt)21221 (Tg21221) to produce APP/PS1-rTg4510 or APP/PS1-rTg21221 mice with the experimental, tau-expressing genotypes plus mice negative for either the responder or transactivator transgene that do not express any human tau. All of the same sex offspring of these crosses share the FVBB6F1 background and are genetically identical to one another except for the transgene arrays that they carry. Both male and female mice were used and three different ages were studied: young (3- to 4-months), adult (6- to 12-months) and aged (17-to 24-months). All animal experiments were approved by the Massachusetts General Hospital's and McLaughlin Research Institute's Institutional Animal Care and Use Committees.

Wild animals

The study did not involve wild animals.

Field-collected samples

The study did not involve samples collected from the field.